J Neural Transm (2007) 114: 1559–1567
DOI 10.1007/s00702-007-0789-2
Printed in The Netherlands

Journal of Neural Transmission

In parkinsonian substantia nigra, α-synuclein is modified by acrolein, a lipid-peroxidation product, and accumulates in the dopamine neurons with inhibition of proteasome activity

M. Shamoto-Nagai[1], W. Maruyama[1], Y. Hashizume[2], M. Yoshida[2], T. Osawa[3], P. Riederer[4], M. Naoi[5]

[1] National Center for Geriatrics and Gerontology, Department of Geriatric Medicine, Obu, Aichi, Japan
[2] Institute for Medical Science of Ageing, Aichi Medical University, Nagakute-cho, Aichi, Japan
[3] Laboratory of Food and Biodynamics, Nagoya University Graduate School of Bioagricultural Sciences, Nagoya, Aichi, Japan
[4] Clinical Neurochemistry and NPF Center of Excellence Laboratories, Department of Psychiatry and Psychotherapy, University of Würzburg, Würzburg, Germany
[5] Department of Neurosciences, Gifu International Institute of Biotechnology, Kakamigahara, Gifu, Japan

Received 22 April 2007; Accepted 28 June 2007; Published online 10 August 2007

Summary. α-Synuclein (αSYN) plays a central role in the neural degeneration of Parkinson's disease (PD) through its conformational change. In PD, αSYN, released from the membrane, accumulates in the cytoplasm and forms Lewy body. However, the mechanism behind the translocation and conformational change of αSYN leading to the cell death has not been well elucidated. This paper reports that in the dopamine neurons of the substantia nigra containing neuromelanin from PD patients, αSYN was modified with acrolein (ACR), an aldehyde product of lipid peroxidation. Histopathological observation confirmed the co-localization of protein immunoreactive to anti-αSYN and ACR antibody. By Western blot analyses of samples precipitated with either anti-αSYN or anti-ACR antibody, increase in ACR-modified αSYN was confirmed in PD brain. Modification of recombinant αSYN by ACR enhanced its oligomerization, and at higher ACR concentrations αSYN was fragmented and polymerized forming a smear pattern in SDS-PAGE. ACR reduced 20S proteasome activity through the direct modification of the proteasome proteins and the production of polymerized ACR-modified proteins, which inhibited proteasome activity *in vitro*. These results suggest that ACR may initiate vicious cycle of modification and aggregation of proteins, including αSYN, and impaired proteolysis system, to cause neuronal death in PD.

Keywords: Acrolein; α-synuclein; Parkinson's disease; protein aggregation; dopamine neuron; proteasome

Abbreviations

ACR acrolein
αSYN α-synuclein
HNE 4-hydroxy-2-nonenal
PD Parkinson's disease
RNS reactive nitrogen species
ROS reactive oxygen species
UPS ubiquitin-proteasome system

Correspondence: Wakako Maruyama, National Center for Geriatrics and Gerontology, Department of Geriatric Medicine, Obu, Aichi 474-8511, Japan
e-mail: maruyama@nils.go.jp

Introduction

Accumulation of aggregated denatured proteins is a common feature in age-dependent neurodegenerative disorders, such as Parkinson's disease (PD), Alzheimer's disease and amyotrophic lateral sclerosis (Trojanowski and Lee 2000). In PD, α-synuclein (αSYN) is the major component of Lewy bodies and neurites, the pathological hallmarks of PD (Spillantini et al. 1997), and the filamentous form of αSYN accumulates in degenerating dopamine neurons (Irizarry et al. 1998; Fujiwara et al. 2002). Aggregation and fibril formation of αSYN are now considered to play a role also in the pathogenesis of other α-synucleinopathies, such as dementia with Lewy bodies and multiple system atrophy. In the rare case of early-onset, autosomal dominant forms of PD, the mutations of αSYN gene, A53T (Polymeropoulos et al. 1997), A30P (Kruger et al. 1998) and E46K (Zarranz et al. 2004) and the gene triplication (Singleton et al. 2003) were identified as possible etiologic factors. In transgenic animals expressing wild and mutated human αSYN, a PD-like phenotype was observed, including degeneration of dopamine neurons, formation of αSYN-containing inclusions and the onset of motor dysfunction (Feany and Bender 2000; Masliah et al. 2000).

These results indicate that αSYN is also involved in the pathogenesis of the sporadic PD through the excess production or the conformational change similar to mutated αSYN (Polymeropoulos et al. 1997; Singleton et al. 2003). However, it remains to be elucidated how αSYN is involved in pathogenic factors, such as increased oxidative stress, mitochondrial dysfunction and impaired ubiquitine-proteasome function to induce the selective cell death in nigral dopamine neurons.

αSYN is a small cytosolic protein of 14 kDa and enriched in presynaptic nerve terminal of the brain, but its physiological function remains unknown. The secondary structure of αSYN depends on the environment. αSYN exists in a random-coil structure in aqueous solution, forms α-helical structure upon binding to phospholipids vesicle and β-sheet structure in soluble fibrils. The amino-terminal region (residues 7–87) of αSYN contains a series of amphipathetic α-helical domains composed of 6 repeats of the amino acid sequence, KTK(E/Q)GV, which is similar to the repeats characteristic for A_2 apolipoproteins, and is associated with lipid membranes (Jo et al. 2000). The central region (residues 61–95) is very hydrophobic and is the same as the fragments isolated from Alzheimer's disease senile plaques. The carboxyl-terminal regions are rich in glutamate and quite acidic. The secondary and primary structure of αSYN account for the interaction with other cellular components.

Point mutation (A30P) of αSYN abolishes the ability to bind to the lipid vesicles (Clayton and George 1999), which will break the equilibrium between membrane-bound and free αSYN and cause the aggregation of free αSYN. Another mutation (A53T) of αSYN does not affect the lipid binding capacity, but reduces synaptosomal membrane fluidity (Jo et al. 2004). Actually, mutated αSYN accelerates the formation of more toxic protofibril (prefibrillar oligomer), but not of fibril (Li et al. 2002). These results suggest that the altered interactions between αSYN and lipids may contribute to the cell death in PD.

In sporadic PD, post-translational events may affect αSYN conformation to increase filamentous and reactive property similar to those of mutated αSYN. In sporadic PD, increased oxidative stress with generation of reactive oxygen and nitrogen species (ROS and RNS), a well-confirmed risk factor, may modify proteins in the nigro-striatal dopamine neurons, as shown by the increased immunoreactivity against protein-bound 4-hydroxy-2-nonenal (HNE), an aldehyde produced by lipid peroxidation, in the nigral neurons of PD brains (Yoritaka et al. 1996). In addition, 3-nitrotyrosine, a product of tyrosine with peroxynitrite, was detected in αSYN in Lewy bodies (Giasson et al. 2000). Considering that αSYN plays a role in lipid transport and synaptic membrane biosynthesis through binding to lipid membrane, it may be reasonable to consider that lipid peroxide and produced aldehydes will conjugate with αSYN proteins and change their conformation. Acrolein (ACR) is another reactive aldehyde produced by lipid peroxidation, and ACR and HNE covalently bind to lysine, histidine and cysteine residues of proteins, or nucleotides by the Michael addition. HNE was reported to bind to αSYN at His^{50} *in vitro* (Trostchansky et al. 2006). However, the occurrence of HNE- and ACR-modified αSYN conjugate in the human brain has never been reported. ACR-protein adduct contains an electrophilic center, which induces severe conformational changes in itself and other proteins through intra- and inter-crosslinking (Furuhata et al. 2002; Burcham et al. 2004).

In this paper, we examined whether αSYN is modified with ACR in the brains of parkinsonian patients using the antibody specific against αSYN and ACR, which was prepared by use of a stable ACR-amino acid adduct, N^{ε}-(3-formyl-3,4-dehydropiperidino)-lysine (FDP-lysine) as the antigen (anti-ACR antibody) (Uchida et al. 1998). The existence of αSYN-ACR adduct was also studied by the immunoprecipitation of samples prepared from the substantia nigra of control and parkinsonian patients. The aggregation of ACR-modified proteins was examined using human recombinant αSYN, and effects on the proteasome activity was examined using purified proteasome sample and dopaminergic SH-SY5Y cells. The results are discussed in relation to the involvement of αSYN-ACR adduct formation in the production of reactive αSYN oligomer (Lee and Lee 2002) which may induce the cell death of dopamine neurons in PD.

Material and methods

Materials

Autopsied brains from 4 PD patients (age 72 ± 9.8 years, M/F = 2/2) and 4 controls without neurological diseases (age 76 ± 3.4 years, M/F = 1/3) were used for the immunochemical analysis. The substantia nigra from brains of 2 control and 4 parkinsonian patients was isolated by punching out, and stored at −80°C until analysis. The protocol of brain sample analysis was approved by the ethical committee of Aichi Medical University (for formalin-fixed samples) and that of University of Würzburg, (for frozen samples). ATP, lactacystin and ACR were purchased from Sigma-Aldrich (St. Louis, USA); purified 20S proteasome and human recombinant αSYN from BIOMOL International (Butler Pike, PA, USA). 7-Amino-4-methyl-coumarin (AMC) and a fluorescent substrate for proteasome, carbobenzoxy-L-leucyl-L-leucyl-L-valyl-L-tyrosine-4-methyl-coumaryl-7-amide (Z-LLVY-MCA) were purchased from Peptide Institute (Osaka, Japan). Anti-ACR monoclonal antibody was purchased from NOF (Tokyo, Japan); polyclonal antibody against C-terminal fragment of αSYN from IBL (Takasaki, Japan) for fluoromicroscopy and from Sigma-Aldrich (St. Louis,

USA) for confocal microscopy. Alexa fluor® antibodies were purchased from Molecular Probes (Eugene, OR, USA).

Immunostaining of human brain samples

Paraffin-embedded human midbrain sections containing the substantia nigra were used for immuno-histochemical observation for ACR-adduct protein and αSYN, using DAKO immunostaining kit (DAKO, Kyoto, Japan), as reported (Calingasan et al. 1999). The 8-μm-thick transverse sections were heated at 60°C for 60 min, deparaffinized and hydrated with graded ethanol solution, then rinsed in 50 mM Tris–HCl, pH 7.5 (Duda et al. 2000). The sample was incubated with the anti-αSYN rabbit polyclonal antibody (IBL) (1:50) and anti-ACR mouse monoclonal antibody (1:100), then with the biotinylated anti-mouse secondary antibody (DAKO, 1:200) for 45 min at the room temperature. The sample was further incubated with Alexa fluor® 488 anti-rabbit secondary antibody (1:200) and streptavidin-Alexa Fluor® 594 conjugate (1:200) for 45 min. Green fluorescence of Alexa fluor® 488 for αSYN and red fluorescence of Alexa flour® 594 for ACR were observed by use of a fluorescence microscope, Olympus BX60 (Olympus, Tokyo, Japan). Nuclei were stained with hematoxylin. Fifty neuromelanin-containing neurons were examined by fluoromicroscopy whether they were stained positively for either αSYN or ACR, or for both of them in the substantia nigra of 4 parkinsonian brains and 4 control brains.

For confocal microscopy observation, the samples were deparaffinized and hydrated, then, incubated with anti-αSYN rabbit polyclonal antibody (Sigma-Aldrich) (1:50) and anti-ACR mouse monoclonal antibody (1:100) for 45 min. The samples were incubated with Alexa-fluore® 555 anti-rabbit secondary antibody (1:200) and streptavidine-Alexa fluor® 488 conjugated (1:200) for 45 min. Green fluoresscence of Alexa fluor® 488 for ACR and red fluorescent of Alexa fluor® 555 for αSYN were observed by use of the LSM 510 system (Carl Zeiss Microinaging, Jena, Germany).

Immunoprecipitation of ACR-modified αSYN in samples from human brains

Immunoprecipitation of the samples from control and parkinsonian brains was performed, as reported previously (Shamoto-Nagai et al. 2003). In short, 50–100 mg of human brain was lyzed in about 8-fold volume of the lysis buffer [10 mM Tris–HCl buffer, pH 7.5, containing 150 mM NaCl, 1 mM EDTA, 0.2 mM phenylmethylsulfonyl fluoride, 1% Triton X-100 and protease inhibitor cocktail (Roche Diagnostics, Indianapolis, Indiana, USA)]. The lysate (2 mg protein) was incubated with 5 μl of anti-αSYN antibody (primary antibody) (IBL, 10 μg protein) at 4°C overnight. The mixture was then treated with 25 μl of protein A-Magnetic beads (New England BioLabs, Ipswich, MA, USA) and incubated at 4°C for 1 h. The mixture was applied to magnetic field and the beads were washed with the lysis buffer for three times. The beads were suspended in the Laemmli sample buffer, boiled for 5 min at 98°C, and the solubilized sample of αSYN and its binding proteins were applied to SDS-PAGE for immunoblotting with anti-αSYN or anti-ACR antibodies. The relative density of the bands positive both αSYN and ACR was quantified by NIH imaging software.

Determination of αSYN modification and aggregation by ACR

αSYN (2.5 μM in the final concentration) dissolved in 10 mM Tris–HCl buffer, pH 7.5, was incubated in the presence of 0.5, 1, 5, or 10 mM of ACR at 37°C for 20 h. Then, the equal volume of the Laemmli buffer was added to the reaction mixture and the sample was boiled at 100°C for 5 min. The mixture of ACR with αSYN without the incubation was used as a blank. The sample was subjected to Western blot analysis, by SDS-PAGE on 5–20% gradient gel (Wako Pure Chemical Industries, Osaka, Japan), blotted onto PVDF membrane and stained with the anti-αSYN or anti-ACR antibody.

The effect of ACR on 20S proteasome in vitro

The effect of ACR on the activity of 20S proteasome was estimated *in vitro*. The enzyme preparation (50 μg protein) or purified 20S proteasome (100 μg, BIOMOL) was incubated with or without 10 mM ACR in the reaction mixture [50 mM Tris–HCl buffer, pH 8.0, containing 1 mM dithiothreitol (DTT) and 0.5 mM EDTA 2Na] for 30 min at 37°C. Then, the substrate Z-LLVY-MCA (50 μM in the final concentration) was added to the reaction mixture and incubated for another 30 min. The reaction was terminated by adding the same volume of 1% SDS in 100 mM Tris–HCl buffer, pH 8.0. The fluorescence intensity of AMC cleaved by 20S proteasome was quantified at 440 nm with excitation at 380 nm using a Shimadzu spectrofluorometer RF-5300. The activity of the proteasome was expressed as pmol AMC cleaved per min per mg protein (Shamoto-Nagai et al. 2003). The effect of ACR on 20S proteasome derived from SH-SY5Y cells were examined also. The cells were mechanically harvested and washed twice in phosphate-buffered saline (PBS). Then, the cells were homogenized in PBS and centrifuged at 14,000 *g* for 60 min. Glycerol was added to the supernatant to be 20% in volume, which was used as an enzyme preparation for measurement of 20S proteasome activity. Then, the enzyme preparation was treated with ACR in the same way of the purified 20S proteasome protein.

The production of ACR-adducted proteins was estimated by use of SDS-PAGE followed by immunoblotting as described in the above section.

Effect of ACR-modified αSYN on 20S proteasome activity in vitro

The effect of the αSYN modified by ACR on 20S proteasome was examined further using ACR-modified αSYN. αSYN dissolved in PBS (1 mg/ml) was incubated in the absence or presence of 5 μM to 5 mM ACR at 37°C for 20 h. Conjugation of ACR to αSYN was confirmed by SDS-PAGE using 5–20% gradient gel and immunoblotting with the antibody against αSYN or ACR. The purified 20S proteasome (100 μg) was incubated for 30 min in the absence or presence of 10 μg of native αSYN, or αSYN incubated with 50, 500 μM, and 5 mM ACR. The activity of chymotrypsin-like 20S proteasome was quantified using Z-LLVY-MCA as a substrate as described above. As a positive control, the effect of 10 μM lactacystin (Lac), an inhibitor of 20S proteasome, was examined.

Statistics

Experiments were repeated at least 4 times, and the data were expressed as mean ± SD. Difference was statistically evaluated by analysis of variance (ANOVA), followed by Sheffe's *F*-test. A p value less than 0.05 is considered to be statistically significant.

Results

Detection of ACR-modified αSYN in the cytoplasm of neuromelanin-containing dopamine neurons from PD brains

By histopathological observation, αSYN was detected in the dopamine neurons containing neuromelanin in the substantia nigra of PD patients (Fig. 1, A-I and -II). Proteins immunoreactive to anti-αSYN antibody were found in the cytoplasm (Fig. 1, B-I) and mostly co-localized with those stained with anti-ACR antibody. In Table 1, the number of positively immunoreactive neurons was expressed as the percentage of the neuromelanin-containing neurons. In PD, the number of neurons positive for both αSYN and

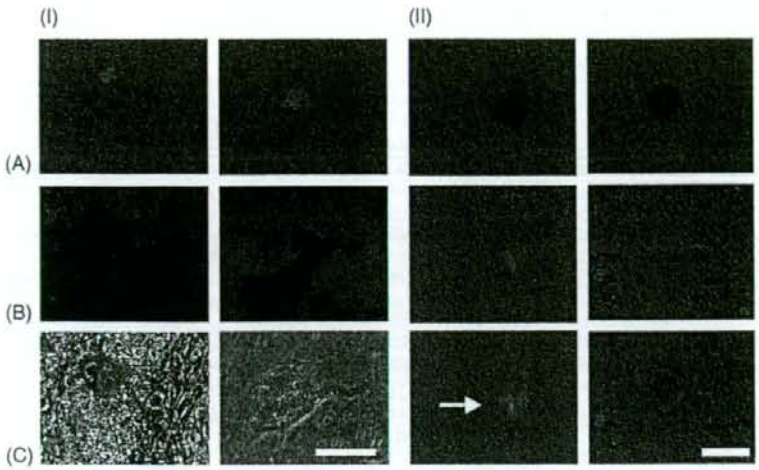

Fig. 1. Co-localization of αSYN and ACR immunoreactivity in the dopamine neurons of the substantia nigra from control and PD patients. Immunoreactivity of αSYN to anti-ACR antibody in dopamine neurons of PD brains. (I) Fluorescence microscopic obsevation The immunoreactivity of αSYN (**A**) was observed in the cytosol and in Lewy body, but that of ACR (**B**) was not prominent in Lewy bodies. (**C**) Phase contrast. Bar = 10 μm. (II) Confocal microscopic observation. The dopaminergic neurons in PD with Lewy bodies, were stained with αSYN (**A**) and ACR (**B**). There is co-localization of ACR and αSYN in Lewy body (*white arrow*, in **C**). Bar = 10 μm

Table 1. *Incidence of ACR- and αSYN-positive neuromelanin-containing dopamine neurons in the substantia nigra of PD and control patients*

	ACR	αSYN	ACR and αSYN
PD ($n=4$)	$37.9 \pm 13.7^*$	$47.4 \pm 15.8^*$	$28.4 \pm 26.7^*$
Control ($n=4$)	8.6 ± 3.8	13.1 ± 8.6	3.4 ± 4.1

Formalin-fixed sections of the human midbrain were stained with antibodies against ACR and αSYN as described in the Material and methods. The percentages of the neuromelanin-containing dopamine neurons immunoreactive to antibody against ACR, αSYN, or both of them are expressed as mean and SD. $^*p < 0.05$ by unpaired p-test.

ACR was 28.4% of neuromelanin-containing neurons, whereas in the control brain, only 3.4%. The cells without neuromelanin were neither immunopositive to αSYN or ACR (data, not shown). The microscopic observation was confirmed using another antibody against αSYN and confocal microscopy (Fig. 1, A-II and B-II). The most of the cases, ACR-positive proteins were observed in the cytoplasm but small number of Lewy bodies which are double positive for αSyn and ACR was observed (white arrow). The co-localization of ACR and αSYN was confirmed also under these conditions (Fig.1, C-II).

Increased formation of ACR-conjugated αSYN was further proved by the immuno-precipitation of αSYN protein. As shown in Fig. 2, in samples from PD patients the protein bands corresponding to αSYN (black arrow) were more intensively stained with the anti-ACR antibody. Fig. 2A shows that anti-αSYN polyclonal antibody used here stained many protein bands, in addition to the band corresponding to αSYN monomer of 14 kDa. In PD brain, intensitiy of ACR-positive proteins was increased (white arrow), and most of them corresponded with those stained with αSYN antibody (Fig. 2B). Figure 2C shows the quantitative analyses of the immunoreactivity against ACR in protein band corresponding to αSYN monomer of 14 kDa, as the relative ratio of the density stained with the anti-ACR against that with anti-αSYN antibody. The ACR-modified αSYN significantly increased in the substantia nigra sample from all 4 PD patients.

ACR induced oligomerization and aggregation of αSYN in vitro

The effects of ACR on tertiary structure of αSYN were studied *in vitro* using recombinant human αSYN. As shown in Fig. 3, in αSYN samples treated with ACR for 20 h, the band corresponding αSYN monomer with a molecular mass of 14 kDa become broader and reactive to anti-ACR antibody, indicating modification of αSYN by ACR (black arrow). In addition, oligomerized and aggregated αSYN was enhanced in the sample treated with ACR (white arrow). αSYN treated with 10 mM ACR was detected as highly polymerized with random molecular mass, suggesting the destruction and fragmentation of αSYN. The αSYN aggregation was dose-dependent to ACR concentration, and the polymerization and aggregation were not observed in αSYN-ACR mixture before incubation (0 time samples). Figure 3C shows how the ACR modification induces cross-reaction of protein and polymerization.

ACR reduced the activity of 20S proteasome in vitro

Effect of ACR on the activity and high structure of 20S proteasome in the cytoplasmic fraction of the purified sample and SH-SY5Y cells were examined *in vitro*. ACR markedly reduced the activity of 20S proteasome in both

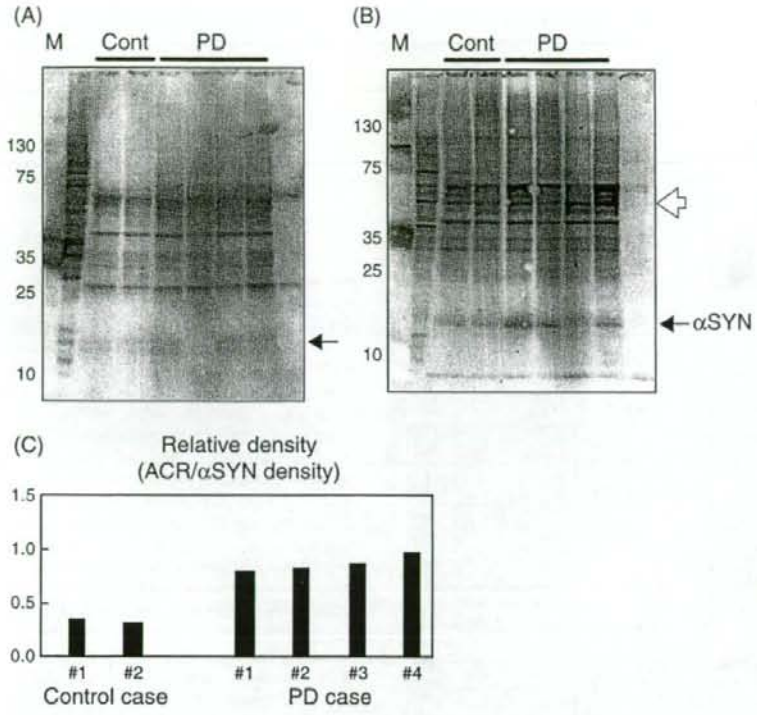

Fig. 2. Modification of αSYN by ACR in the PD brains. Samples from the substantia nigra of control (*Cont*) and PD patients (*PD*) were homogenized and immunoprecipitated with antibody against αSYN. The samples were subjected to SDS-PAGE and detected using anti-αSYN (**A**) and anti-ACR antibody (**B**) as described in the Material and methods. (**C**) The relative density of immuno-staining of the protein band stained with anti-ACR antibody against that with anti-αSYN antibody was assessed using the image analysis software. αSYN in samples prepared from PD brains was more markedly stained against anti-ACR antibody (*black arrow*). In PD brain samples, the increase of ACR-modified protein was observed (*white arrow*) (**B**)

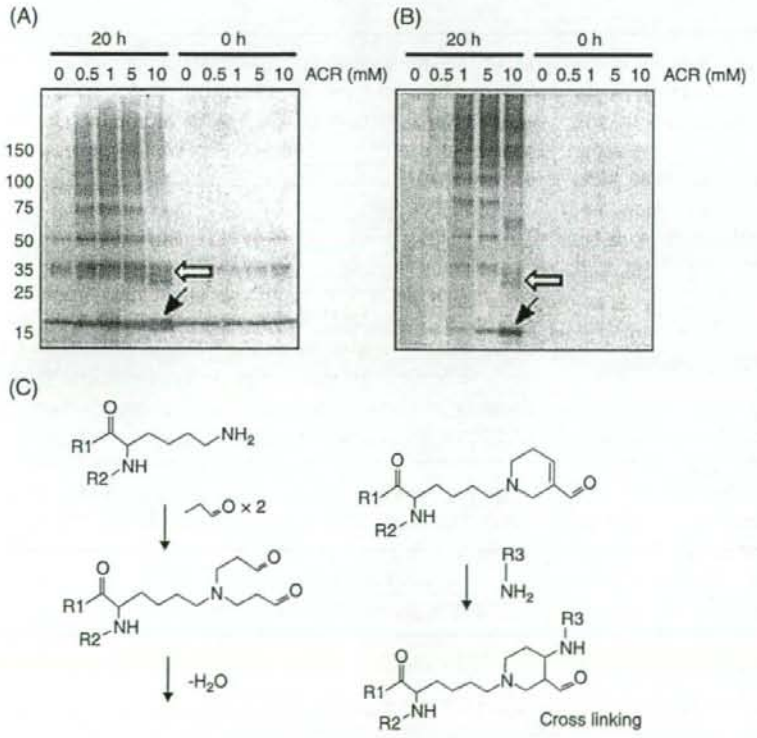

Fig. 3. Oligomerization and aggregation of αSYN induced by ACR-modification. αSYN (2.5 μM) was incubated in the presence of 0.5, 1, 5, or 10 mM of ACR at 37°C for 20 h as described in the Material and methods. Then, the samples were separated by SDS-PAGE and blotted using anti-αSYN or anti-ACR antibody. (**A**) Immunoblotting using anti-αSYN antibody. (**B**) Immunoblotting using anti-ACR antibody. *Balck arrow* αSYN monomer was modified by ACR. *White arrow* in the sample incubated with ACR, oligomerization of αSYN was detected. (**C**) The scheme of chain reaction of ACR with amino acids to produce cross-linking of proteins

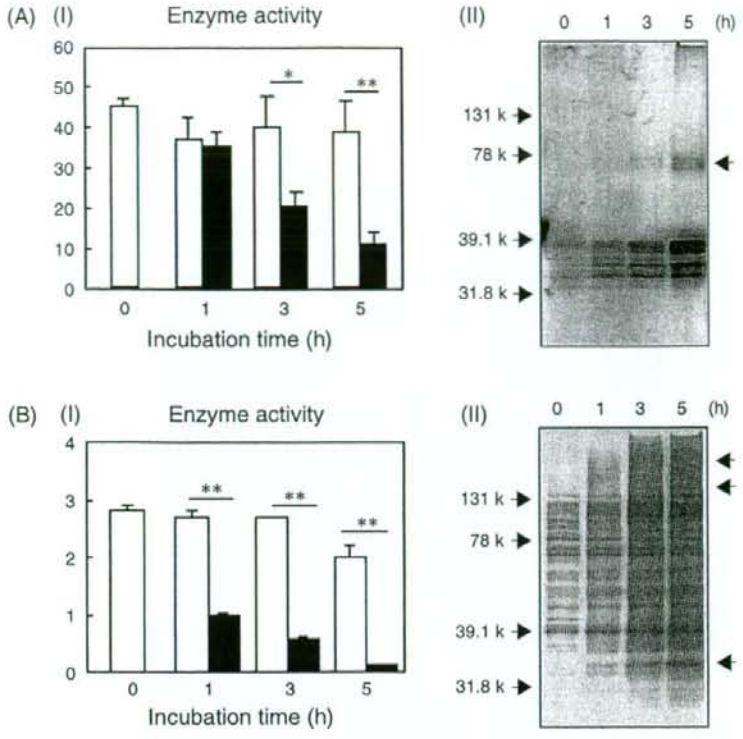

Fig. 4. Modification of 20S proteasome by ACR and reduction of the enzyme activity *in vitro*. The enzyme sample prepared from the purified 20S proteasome (A) or cytoplasmic fraction of SH-SY5Y cells (B) was incubated without or with 1 mM of ACR solution for 1 to 5 h. (A-I) and (B-I): Chymotrypsin-like activity of 20S proteasome was measured fluorometrically using LLVY-AMC as a substrate, as described in Material and methods. The column and bar represent the mean and SD of 4 independent experiments. Difference from the activity in control treated without ACR was significant ($^{**}p<0.01$) by ANOVA. (A-II) and (B-II): The samples are separated by SDS-PAGE and visualized with antibody against ACR. After incubation of the cytosol with ACR, increased number of the proteins immunoreactive to anti-ACR antibody was observed, indicating that ACR adducted multiple proteins [(B-II)]. Adduct formation of ACR with 20S proteasome was identified by use of purified enzyme sample [(A-II)]

the samples (Fig. 4, A-I and B-I). The inhibition of the activity was more potent in the cytoplasmic enzyme preparation than in the purified enzyme. The activity of 20S proteasome was virtually undetectable in the cytoplasmic enzyme preparation after 5 h incubation with 10 mM ACR. By Western blot analysis of the cytoplasmic sample, numerous proteins were modified with ACR (Fig. 4, B-II). The purified 20S proteasome were also modified by ACR with aggregation to high polymers (Fig. 4, A-II).

αSYN conjugated with ACR inhibited 20S proteasome activity in vitro

The direct effect of ACR-modified αSYN on the 20S proteasome activity was examined *in vitro*. After the incubation with ACR, polymerized αSYN conjugated with ACR (ACR-SYN) increased in a dose-dependent way to ACR (Fig. 5A). In the αSYN sample incubated with 5–100 μM ACR, the dimmer, tetramer and higher polymers of aSYN were observed as ladder formation, whereas with 500 μM and 5 mM ACR, αSYN was cleaved and aggregated showing smear pattern (Fig. 5A). As shown in Fig. 5C, αSYN treated with 5 mM of ACR for 20 h inhibited 20S proteasome activity significantly ($p<0.001$). Pre-treatment of 100 μg of enzyme sample with 10 μg ACR-SYN adduct reduced the activity to be $40.0 \pm 4.5\%$ of control. On the other hand, native αSYN did not affect the 20S proteasome activity at all.

Discussion

Our results show that in the substantia nigra from PD patients ACR-modified αSYN accumulates mainly in the cytoplasm of the nigral melanized neurons. Western blot analyses of the lysate immuno-precipitated with anti-αSYN antibody confirmed the increased ACR-modification of αSYN in the substantia nigra of parkinsonian brains. αSYN localizes on the lipid bilayer of the synaptic vesicles and lipid rafts of the presynaptic terminal (Kahle et al. 2000; Zhu et al. 2003; Fortin et al. 2004; Nuscher et al. 2004), and it exists in three conformations: lipid bound α-helices, unfolded in solution and fibrils (Kessler et al. 2003). The protein structure of αSYN contains seven imperfect repeats of 11 amino acids, forming N-terminal α-helices, a central hydrophobic domain and acidic C-terminal rich in glutamate. The primary structures and con-

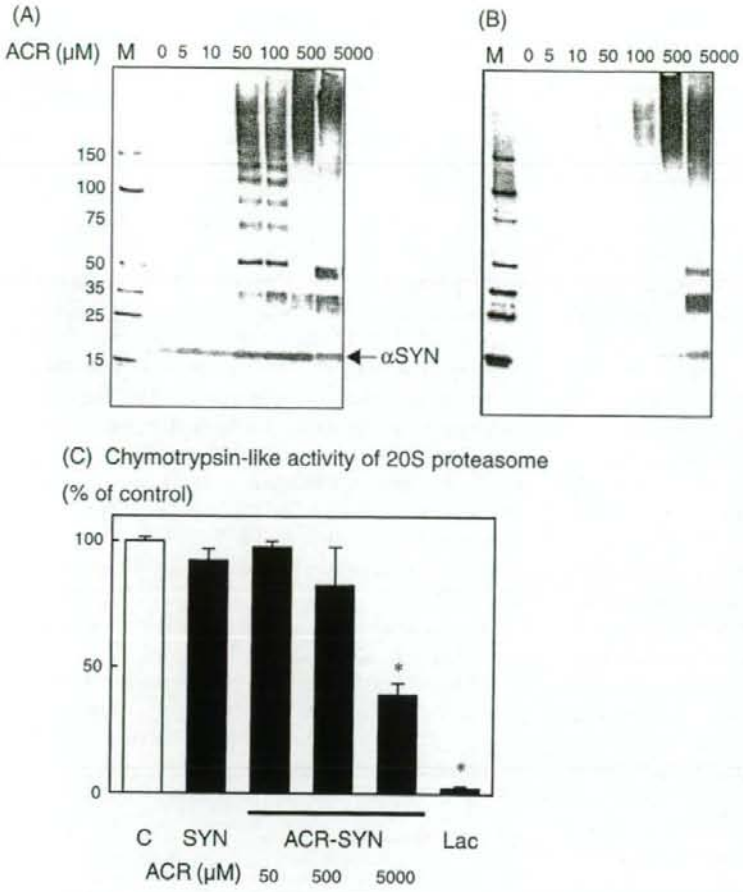

Fig. 5. Inhibition of purified 20S proteasome activity by ACR-modified αSYN (*ACR-SYN*). αSYN was incubated without or with 5 μM to 50 mM ACR for 20 h and the sample was subjected to SDS-PAGE and detected with anti-αSYN antibody (**A**) or anti-ACR antibody (**B**) as described in the Material and methods. αSYN (*arrow*) was conjugated with ACR in a dose-dependent manner. (**C**) The 20S proteasome sample was pre-incubated in the absence or presence of αSYN or αSYN modified by ACR (ACR-SYN) for 30 min. Then, the chymotrypsin-like activity of 20S proteasome was measured using a synthesized substrate, LLVY-AMC. *C* The enzyme sample without αSYN, *SYN* enzyme sample incubated with native αSYN, *ACR-SYN* enzyme sample incubated with ACR-treated αSYN at the indicated concentrations. $^{*}p < 0.001$ compared to control by ANOVA

formation suggest that αSYN may function in protein-membrane, namely protein–lipid, interaction. The interaction of αSYN with lipids has been well confirmed and the association with lipids induced the oligomer formation (Eliezer et al. 2001). The dissociation of αSYN from lipids may transform the primarily random-coil secondary structure to β-sheet rich structure, which promotes protofibril formation in cytoplasm. αSYN oligomer and protofibril are now proposed to be cytotoxic by permeabilization of membranes (Volles et al. 2001; Rochet et al. 2004), increased generation of ROS and RNS (Xu et al. 2002), and elevated levels of αSYN β-sheet (Petrucelli et al. 2002). These results suggest that factors regulating the αSYN conformation, the affinity to lipid layer and the equilibrium between the monomer, oligomer, protofibril and fibril form, may play an important role in the formation of the inclusion body, and the cell death of nigral dopamine neurons.

In addition to αSYN gene mutation, the oxidative modification will induce the conformational changes in αSYN, and its close localization to lipid bilayer suggests the products of lipid peroxidation, aldehydes and radicals, may mediate the oxidative modification. ACR modifies protein by adduct formation with the imidazole group of histidine, amino group of lysine, and sulfhydryl group of cysteine, then ACR undergoes nucleophilic addition at the double bond to form a secondary derivative with the retention of the aldehyde group, resulting in the formation of the Michaelis addition-type ACR-amino acid adducts. ACR modification of histidine and lysine produce further 3-(*N*-imidazole)propanol and N^{ε}-(3-formyl-3,4-dehydropiperidino)-lysine (FDP-lysine), respectively. FDP-lysine reacts with sulfhydril groups to form thioether adducts (Furuhata et al. 2002). This reaction may accelerate the cross linkage of between αSYN and other proteins (Fig. 3C). Even

though the half life of free ACR was very short by *in vitro* and *ex vivo* experiments, ACR modifies protein very effectively in a short time (Uchida et al. 1998). Indeed, incubation of αSYN with ACR rapidly produced aggregated ACR-modified protein (Figs. 3 and 5). Figure 5 shows that ACR at 50 μM already induces αSYN polymerization. At present the exact concentration of ACR in human brain has not been determined, but in rat tissues the HNE concentration was estimated around 3 μM, which increased to 10 μM by oxidative stress (Esterbauer et al. 1990). Considering dysfunction of the UPS in PD, it may be reasonable to consider that ACR even lower concentrations may modify αSYN, resulting in the accumulation in dopamine neurons of aged and parkinsonian brain. In addition, ACR itself inhibits the activity of proteasome, as discussed below.

In oligomerized αSYN, the immunoreactivity against ACR was not prominent compared to αSYN monomer. It may be ascribed to that ACR binding site and/or the recognition site of anti-ACR antibody were not fully any more exposed in aggregated αSYN as in the case of Lewy body. This may explain also the different distribution of ACR- and αSYN-positive cells in neuromelanin-containing neurons, and why only a third of neurons were stained with both the antibodies (Table 1). In addition, conformational changes of ACR modified αSYN into the oligomer, filamentous or insoluble form may explain the limited increase in ACR-αSYN adducts in immuno-precipitated sample from PD patients (Fig. 2).

The possible toxicity of ACR and ACR modified αSYN was studied especially in concern with proteasome activity. Impairment of the proteolysis system has been gathering attention as a mechanism of neuronal cell death in PD. Gene mutation and inactivation of the enzymes of the UPS, including parkin, E3 ubiquitin-ligase (Kitada et al. 1998) and ubiquitin C-terminal hydrolase L1 (Leroy et al. 1998), were identified as pathogenic factors in autosomal recessive familial PD. Also in sporadic cases of PD, reduced activity of 20S proteasome was reported in the striatum (McNaught and Jenner 2001). As shown in Fig. 4, B-I, free ACR markedly reduced 20S proteasome activity in the cytoplasmic enzyme preparation, and the mechanism behind the inhibition of the activity was studied. ACR was found to adduct with many components of 20S proteasome proteins as shown in the purified enzyme proteins incubated with ACR (Fig. 4, A-II). ACR may directly modify the proteasomal proteins, then, induce conformational change with inactivation of the enzyme. It was further demonstrated using purified 20S proteasome, the activity of which was reduced, according to the modification and aggregation of proteasomal protein (Fig. 4, B-II).

Another mechanism of the inhibition is the effect of ACR-adduct proteins on proteasome. Oxidative-modified protein is a substrate and inhibitor of 20S proteasome system (Shringarpure et al. 2003). We found that rotenone, a complex I inhibitor, induced the reduction of 20S proteasome activity and the accumulation of aggregated ACR-modified proteins to induce apoptotic cell death in human neuroblastoma SH-SY5Y cells (Shamoto-Nagai et al. 2003). In that system ACR-modified protein was co-immunoprecipitated with 20S β subunit, the active site of 20S proteasome. In this article ACR-modified proteins was shown to inhibit 20S proteasome activity directly. The relatively weak potency of inhibition by ACR-SYN may be ascribed to that the molecular size of αSYN protein is much larger than that of the synthesized peptide substrate. Proteasome system is composed of a cylinder-like structure and in the hole disentangled proteins are cleaved by enzymes into small peptides. The peptides or protein fragments released from ACR-modified αSYN or other proteins may act as an endogenous inhibitor of the proteasome system.

The modification of αSYN with ACR may initiate the accumulation of abnormal proteins by impairment of the UPS. A vicious cycle of oxidative stress, mitochondrial dysfunction and reduced UPS activity may culminate in neuronal cell death with accumulation of oligometric αSYN in the sporadic form of PD.

Acknowledgements

We thank to Ms. Hiroko Goto for their skilful assistance during this study. This work was supported by a Grant-in-Aid on Scientific Research for Young Researcher (B) (M. S.-N.) and Comprehensive Research on Aging and Health from the Ministry of Health, Labor and Welfare (W. M. and M. N.), and The Promotion of Fundamental Studies in Health Sciences of National Institute of Biomedical Innovation, Japan (W. M).

References

Burcham PC, Fontaine FR, Kaminskas LM, Petersen DR, Pyke SM (2004) Protein adduct-trapping by hydrazinophthalazine drugs: mechanisms of cytoprotection against acrolein-mediated toxicity. Mol Pharmacol 65: 655–664

Calingasan NY, Uchida K, Gibson GE (1999) Protein-bound acrolein: a novel marker of oxidative stress in Alzheimer's disease. J Neurochem 72: 751–756

Clayton DF, George JM (1999) Synucleins in synaptic plasticity and neurodegenerative disorders. J Neurosci Res 58: 120–129

Duda JE, Giasson BI, Chen Q, Gur TL, Hurtig HI, Stern MB, Gollomp SM, Ischiropoulos H, Lee VM, Trojanowski JQ (2000) Widespread nitration of pathological inclusions in neurodegenerative synucleinopathies. Am J Pathol 157: 1439–1445

Eliezer D, Kutluay E, Bussell R Jr, Browne G (2001) Conformational properties of α-synuclein in the free and lipid-associated states. J Mol Biol 307: 1061–1073

Esterbauer H, Eckl P, Ortner A (1990) Possible mutagens derived from lipids and lipid precursors. Mut Res 238: 223–233

Feany MB, Bender WW (2000) A drosophila model of Parkinson's disease. Nature 404: 394–398

Fortin DL, Troyer MD, Nakamura K, Kubo S, Anthony MD, Edwards RH (2004) Lipid rafts mediate the synaptic localization of α-synuclein. J Neurosci 24: 6715–6723

Fujiwara H, Hasegawa M, Dohmae N, Kawashima A, Masliah E, Goldberg MS, Shen J, Takio K, Iwatsubo T (2002) α-Synuclein is phosphorylated in synucleinopathy lesions. Nat Cell Biol 4: 160–164

Furuhata A, Nakamura M, Osawa T, Uchida K (2002) Thiolation of protein-bound carcinogenic aldehyde. An electrophilic acrolein-lysine adduct that covalently binds to thiols. J Biol Chem 31: 27919–27926

Giasson BI, Duda JE, Murray IV, Chen Q, Souza JM, Hurtig HI, Ischiropoulos H, Trojanowski JQ, Lee VM (2000) Oxidative damage linked to neurodegeneration by selective alpha-synuclein nitration in synucleinopathy lesions. Science 290: 985–989

Irizarry MC, Growdon W, Gomez-Isla T, Newell K, George JM, Clayton DF, Hyman BT (1998) Nigral and cortical Lewy bodies and dystrophic nigral neurites in Parkinson's disease and cortical Lewy body disease contain alpha-synuclein immunoreactivity. J Neuropathol Exp Neurol 57: 334–337

Jo E, Darabie AA, Han K, Tandon A, Fraser PE, McLaurin J (2004) α-Synuclein-synaptosomal membrane interactions: implications for fibrillogenesis. Eur J Biochem 271: 3180–3189

Jo E, McLaurin J, Yip CM, St George-Hyslop P, Fraser PE (2000) α-Synuclein membrane interactions and lipid specificity. J Biol Chem 275: 34328–34334

Kahle PJ, Neumann M, Ozmen L, Muller V, Jacobsen H, Schindzielorz A, Okochi M, Leimer U, van Der Putten H, Probst A, Kremmer E, Kretzschmar HA, Haass C (2000) Subcellular localization of wild-type and Parkinson's disease-associated mutant α-synuclein in human and transgenic mouse brain. J Neurosci 20: 6365–6373

Kessler JC, Rochet JC, Lansbury PT Jr (2003) The N-terminal repeat domain of α-synuclein inhibits β-sheet and amyloid fibril formation. Biochemistry 42: 672–678

Kitada T, Asakawa S, Hattori N, Matsumine H, Yamamura Y, Minoshima S, Yokochi M, Mizuno Y, Shimizu N (1998) Mutations in the parkin gene cause autosomal recessive juvenile parkinsonism. Nature 392: 605–608

Kruger R, Kuhn W, Muller T, Woitalla D, Graeber M, Kosel S, Przuntek H, Epplen JT, Schols L, Riess O (1998) Ala30Pro mutation in the gene encoding α-synuclein in Parkinson's disease. Nat Genet 18: 106–108

Lee HJ, Lee SJ (2002) Characterization of cytoplasmic alpha-synuclein aggregates. Fibril formation is tightly linked to the inclusion-forming process in cells. J Biol Chem 277: 48976–48983

Leroy E, Boyer R, Auburger G, Leube B, Ulm G, Mezey E, Harta G, Brownstein MJ, Jonnalagada S, Chernova T, Dehejia A, Lavedan C, Gasser T, Steinbach PJ, Wilkinson KD, Polymeropoulos MH (1998) The ubiquitin pathway in Parkinson's disease. Nature 395: 451–452

Li J, Uversky VN, Fink AL (2002) Conformational behavior of human α-synuclein is modulated by familial Parkinson's disease point mutations, A30P and A53T. Neurotoxicology 23: 553–567

Masliah E, Rockenstein E, Veinbergs I, Mallory M, Hashimoto M, Takeda A, Sagara Y, Sisk A, Mucke L (2000) Dopaminergic loss and inclusion body formation in α-synuclein mice: implications for neurodegenerative disorders. Science 287: 1265–1269

McNaught KS, Jenner P (2001) Proteasomal function is impaired in substantia nigra in Parkinson's disease. Neurosci Lett 297: 191–194

Nuscher B, Kamp F, Mehnert T, Odoy S, Haass C, Kahle PJ, Beyer K (2004) Alpha-synuclein has a high affinity for packing defects in a bilayer membrane: a thermodynamics study. J Biol Chem 279: 21966–21975

Petrucelli L, O'Farrell C, Lockhart PJ, Baptista M, Kehoe K, Vink L, Choi P, Wolozin B, Farrer M, Hardy J, Cookson MR (2002) Parkin protects against the toxicity associated with mutant α-synuclein: proteasome dysfunction selectively affects catecholaminergic neurons. Neuron 36: 1007–1009

Polymeropoulos MH, Lavedan C, Leroy E, Ide SE, Dehejia A, Dutra A, Pike B, Root H, Rubenstein J, Boyer R, Stenroos ES, Chandrasekharappa S, Athanassiadou A, Papapetropoulos T, Johnson WG, Lazzarini AM, Duvoisin RC, Di Iorio G, Golbe LI, Nussbaum RL (1997) Mutation in the α-synuclein gene identified in families with Parkinson's disease. Science 276: 2045–2047

Rochet JC, Outeiro TF, Conway KA, Ding TT, Volles MJ, Lashuel HA, Bieganski RM, Lindquist SL, Lansbury PT (2004) Interactions among α-synuclein, dopamine, and biomembranes: some clues for understanding neurodegeneration in Parkinson's disease. J Mol Neurosci 23: 23–34

Shamoto-Nagai M, Maruyama W, Kato Y, Isobe K, Tanaka M, Naoi M, Osawa T (2003) An inhibitor of mitochondrial complex I, rotenone, inactivates proteasome by oxidative modification and induces aggregation of oxidized proteins in SH-SY5Y cells. J Neurosci Res 74: 589–597

Shringarpure R, Grune T, Mehlhase J, Davies KJ (2003) Ubiquitin conjugation is not required for the degradation of oxidized proteins by proteasome. J Biol Chem 278: 311–318

Singleton AB, Farrer M, Johnson J, Singleton A, Hague S, Kachergus J, Hulihan M, Peuralinna T, Dutra A, Nussbaum R, Lincoln S, Crawley A, Hanson M, Maraganore D, Adler C, Cookson MR, Muenter M, Baptista M, Miller D, Blancato J, Hardy J, Gwinn-Hardy K (2003) α-Synuclein locus triplication causes Parkinson's disease. Science 302: 841

Spillantini MG, Schmidt ML, Lee VM, Trojanowski JQ, Jakes R, Goedert M (1997) α-Synuclein in Lewy bodies. Nature 388: 839–840

Trojanowski JQ, Lee VM (2000) "Fatal attractions" of proteins. A comprehensive hypothetical mechanism underlying Alzheimer's disease and other neurodegenerative disorders. Ann NY Acad Sci 924: 62–67

Trostchansky A, Lind S, Hodara R, Oe T, Blair IA, Ischiropoulos H, Rubbo H, Souza JM (2006) Interaction with phospholipids modulates alpha-synuclein nitration and lipid-protein adduct formation. Biochem J 393: 343–349

Uchida K, Kanematsu M, Sakai K et al (1998) Protein-bound acrolein: potential markers for oxidative stress. Proc Antl Acad Sci USA 95: 4882–4887

Volles MJ, Lee SJ, Rochet JC, Shtilerman MD, Ding TT, Kessler JC, Lansbury PT Jr (2001) Vesicle permeabilization by protofibrillar α-synuclein: implications for the pathogenesis and treatment of Parkinson's disease. Biochemistry 40: 7812–7819

Xu J, Kao SY, Lee FJ, Song W, Jin LW, Yankner BA (2002) Dopamine-dependent neurotoxicity of α-synuclein: a mechanism for selective neurodegeneration in Parkinson disease. Nat Med 8: 600–606

Yoritaka A, Hattori N, Uchida K, Tanaka M, Stadtman ER, Mizuno Y (1996) Immunohistochemical detection of 4-hydroxynonenal protein adducts in Parkinson disease. Proc Natl Acad Sci USA 93: 2696–2701

Zarranz JJ, Alegre J, Gomez-Esteban JC, Lezcano E, Ros R, Ampuero I, Vidal L, Hoenicka J, Rodriguez O, Atares B, Llorens V, Gomez Tortosa E, del Ser T, Munoz DG, de Yebenes JG (2004) The new mutation, E46K, of alpha-synuclein causes Parkinson and Lewy body dementia. Ann Neurol 55: 164–173

Zhu M, Li J, Fink AL (2003) The association of α-synuclein with membranes affects bilayer structure, stability, and fibril formation. J Biol Chem 278: 40186–40197

いるので，DHAが健康の維持に重要だからといって，単独を多量に摂取すると，かえってPUFA全体の代謝を乱すことになる．

■ PUFA摂取には抗酸化物質の共摂取が必須

PUFAの二重結合は活性酸素の攻撃を受け，ペルオキシラディカルを形成しやすい．これを防ぐために，ビタミンC，E，β-カロテン，ポリフェノールなどの抗酸化剤を一緒に摂取することが必要である[14]．

■ PUFAの推薦摂取量

脂肪摂取総量は全エネルギー摂取量の20％～25％の範囲に収め，PUFAの摂取総量は全エネルギーの10％にするのがよいとされている．

おわりに

最近メタボリックシンドロームの防止のために脂肪の摂食を避ける傾向にある．しかし，n-3系とn-6系のPUFAは健康の維持に欠かすことのできない重要な機能をもつうえに，栄養学うえ必ず摂取しなければならない必須脂肪酸(EFF)[*1]である．

ただし，n-6系のPUFAは過剰になると炎症，血小板凝集などにみられるように病的現象の発現と密接な関係をもつことから，重要性が見逃されている傾向がある．n-6系とn-3系PUFAは同じ酵素群によって代謝されるため，一方の量が多いと，他方の欠乏が起こる．そのことが，たとえばDHAとAAを単純に比較した場合にAAの負の面が浮き彫りにされる．今後は，異なるn-6/n-3をもつPUFAを含む食事を与えて，AAなどn-6系のPUFAの機能を見直す必要があると思われる．

＊1：上述のように，厳密な意味ではALAとLAがEFFに当たる．また，エイコサノイド類の発見に至るまでの経緯からAAを加えて3種のPUFAがEFFとされてきたこともある．しかし，最近ではΔ^6不飽和酵素の活性が制限されているため，たとえば，n-3系のPUFAを供給するのにALAよりむしろEPAやDHAを与えると効率がよいという意味で，n-3系，n-6系のPUFAのすべてをEFFとするのが趨勢である．

文献

1) Gurr MI, Harwood JL, Frayn KN(Eds.). Lipid Biochemistry An Introduction, 5 th : Backwell Science ; 2002.
2) 中川八郎．脳に磨きをかける必須脂肪酸：ケイ・ディー・ネオブック；2002.
3) Whelan J, Rust C, Innovative dietary sources of N-fatty acids. Annu Rev Nutr 2006 ; 26 : 75-103.
4) Mitchell DC, Litman BJ. Modulation of receptor signaling by phospholipid acyl chain composition. In : Mostofsky DI, Yehuda S, Salem Jr. N, editors. Fatty Acids Physiological Behavioral Fuctions : Humana Press ; 2001. p. 23-40.
5) Sampath H, Ntambi JM. Polyunsaturated fatty acid regulation of genes of lipid metabolism. Annu Rev Nutr 2005 ; 25 : 317-40.
6) Postic C, Dentin R, D. Denechoud P-D, Girard J. ChREBP, a transcriptional regulator of glucose and lipid metabolism. Annu Rev Nutr 2007 ; 27 : 179-62.
7) Tsukada H, Kakiuchi T, Fukumoto D, Nishiyama S, Koga K. Docosahexanoic acid (DHA) improves the age-related impairment of the coupling mechanism between activation and functional cerebral blood flow response : A PET study with microdialysis in the awake monkeys. Brain Res 2000 ; 862 : 180-6.
8) 井原康夫，植木　彰，ボケを防ぐ本：マキノ出版；2000.
9) Otsuka M, Yamaguchi Y, Ueki A. Similarities and differences between Alzheimer's disease and vascular dementia from the viewpoint of nutrition. Annu NY Acad Sci 2002 ; 977 : 155-61.
10) Wijendran V, Hayes KC. Dietary N-6 and N-3 fatty acid balance and cardiovasuclar health. Annu Rev Nutr 2004 ; 24 : 597-615.
11) Li Q, Wang M, Tan L, Wang C et al. Docosahexaenoic acid changes lipid composition and interleukin-2 receptor signaling in membrane rafts. J Lipid Res 2005 ; 46 : 1904-13.
12) Fritsche K. Fatty acids as modulators of the Immune Response. Annu Rev Nutr 2006 ; 26 : 45-73.
13) Nakamura NT,Nara TY. Structure, function, and dietary regulation of delta 6, delta 5, and delta 9 desaturase. Annu Rev Nutr 2004 ; 24 : 345-76.
14) Kan I, Melamed E, Offen D, Green P. Docosahexaenoic acid and arachidonic acid are fundamental supplements for the induction of neuronal differentiation. J Lipd Res 2007 ; 48 : 513-17.
15) 中川八郎，脳を鍛えて健康長寿―百歳時代を演出する還社医学への誘い：共立出版社；2000.

野菜(植物性食品)摂取の効果

国立長寿医療センター研究所 老年病研究部
丸山和佳子 *Maruyama, Wakako*

keyword
ビタミン，ファイトケミカル，抗酸化機能，遺伝子発現制御

はじめに

野菜（植物性食品）は食品の重要な要素であるとともに，必須栄養素を含む．それに加え，野菜に含まれる種々の成分が脳の老化，老年病を防御する可能性について注目されている．近年，野菜の摂取が脳の老化を防ぎ，老化にともなう神経変性疾患であるアルツハイマー病やパーキンソン病の発症率を低下させることが疫学的に報告された．

本稿では野菜と脳の老化をめぐる最近のトピックを中心に概説する．もちろん，これらのすべてが証明されたわけではなく，今後の研究が待たれる．

野菜に含まれる微量機能性成分

栄養素（生体の維持に必須な化学物質で食物から摂取されるもの．たんぱく質，脂質，炭水化物の三大栄養素にビタミン，ミネラルを加えたものを五大栄養素という）のなかでもビタミンは，野菜から摂取されるものが大部分である．そのなかでもビタミンCやビタミンEのように直接的に抗酸化作用を有することや，葉酸，ビタミンB_{12}，B_6のように認知症のリスクファクターであるホモシステインの代謝を行うことで，認知症発症を抑制することが期待されているビタミンも多い．

野菜にはいわゆる栄養素や繊維のほかに種々の色素，スパイスなどの微量成分が含まれる．これらの微量成分はその欠乏によっても欠乏症をきたすことがなく，生体の維持に必須ではないためビタミンではない．しかしこれらの一部は薬理作用をもち，薬品，民間薬として使用されている．それだけでなくこれらの日常摂取により疾病の発症を抑制することが期待され，その成分の多くはファイト(＝ギリシャ語で植物)ケミカル（化学物質）と呼ばれる（表1）．

認知症モデルに対する野菜由来成分の効果

ヒト認知症の代表例としてアルツハイマー病がある．高齢化が進むわが国においては年々その患者数が増加しており，65歳以上の高齢者の5％が本疾患に罹患するとされる．アルツハイマー病の真の病因は不明であるが，脳内にベータアミロイド（Aβ）と呼ばれる構造異常蛋白質が凝集し，蓄積することが神経細胞死の直接の引き金となっているとの仮説が広く受け入れられている（アミロイド仮説）．事実，Aβの前駆物質であるamyloid precursor protein (APP)の変異により，アルツハイマー病と同様な病理変化がもたらされることは本仮説を支持するものである（図1）．

APP遺伝子にヒトと同様な変異を起こした

表1　ファイトケミカルの代表例とそれを含む植物性食品

ポリフェノール	イソフラボン類	大豆
	アントシアニン	ブルーベリー
	レスベラトロール	赤ワイン
	カテキン類	緑茶
	クルクミン	ウコン
	フラバノン類	柑橘類
	リグナン類	ごま
有機硫黄化合物	スルフォラファン	ブロコッリー，キャベツ
	アリシン	にんにく
テルペノイド	ルテイン	ほうれんそう
	リコペン	トマト
	beta-クリプトキサンチン	柑橘類
	カプサイシン	とうがらし
糖関連化合物	beta-グルカン	きのこ
	ペクチン	りんご

遺伝子改変マウスの脳にはAβの蓄積が認められる．近年，Aβに対する免疫を賦活することで脳内のAβ凝集体(老人斑)が減少することが報告され，注目を集めている[1]．現在，世界各国でヒトに対するAβ免疫療法が試みられているが，副作用（脳炎など）の問題もあり，いまだ実用化はなされていない．一方，野菜由来の食品成分のなかでもポリフェノールであるクルクミン[2]やレスベラトロール[3]，カテキン[4]などがAPP遺伝子改変マウスの脳内の老人斑を減少させたり，Aβの繊維化を抑制する[5]との知見が得られている．これら食品由来成分はAβの合成を抑制したり，あるいはAβの凝集を抑制することで脳内Aβ蓄積を減少させたと考えられるが，詳細なメカニズムは不明である．また，ヒトにおいても同様な効果が得られるかどうかはわかっていない．

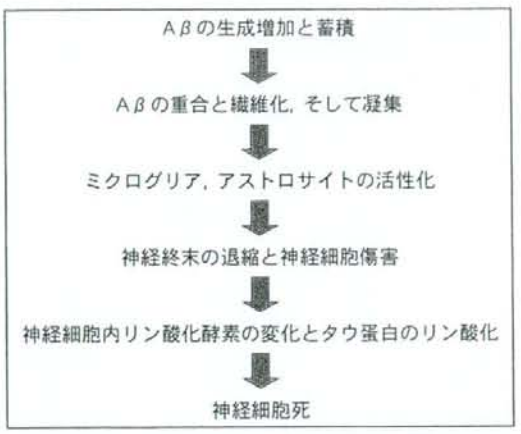

図1　アルツハイマー病のアミロイド仮説
最初になんらかの原因（遺伝子変異，老化，酸化ストレスなど）でベータアミロイド(Aβ)の増加と蓄積が起こり，細胞死のカスケードが起動される．

ヒト認知症に対する野菜成分の効果

ヒト認知症に対する野菜成分の効果を検証するアプローチとしては2つの方法論がある．疫学的研究と，介入研究である．前者はいわゆる観察研究であり，認知症を発症した群と発症していない群を比較し，生活習慣，遺伝的背景などに有意差があるか検定する横断研究，多数例からなるコホートを追跡し，そのなかで認知症を発症した群とそうでない群を比較する縦断研究がある．横断研究は結果が迅速に得られるという利点があるが，世代間の差（生活習慣の変化など）のバイアスがかかりやすいという問題点がある．縦断研究はより正確なデータが得られるものの，解析のためのデータを得るためには膨大な時間と手間がかかるという難点がある．

一方，介入研究は基本的に薬剤開発で用いられる手法と同様な方法論が使用されることが多

表2　疫学研究と介入研究の差

	介入研究（RCT）	疫学研究
評価対象	精製標品（薬剤）	複合品（食品），ライフスタイル
期間	短期（数カ月―数年）	長期（数十年）
対象	疾病患者	コホート （一般地域住民のことが多い）
評価基準	疾病の進行抑制，治癒	疾病発症頻度の抑制

い．認知症を発症した患者を同質な2群に分け，有効と思われる成分を投与された群と偽薬（プラセボ）を与えられた群で症状の進行を比較する（randomized controlled study = RCT）（表2）．

これまでの研究では，疫学研究では野菜摂取の抗認知症効果を示す多くの結果が報告されている[6,7]一方，介入研究のほとんどは失敗に終わっている[8]．この原因は，食品由来成分は薬剤のような強力な作用をもたないため，短期的な治療効果というより長期的な予防効果を検討するための研究デザインが必要なためではないかと考えられる．

野菜由来の微量成分の抗認知症作用のメカニズム

■抗酸化作用

アルツハイマー病などの老年性認知症の最大のリスクファクターは老化である．“老化のフリーラジカル説”[9]は広く受け入れられている概念ではあるが，その実態はなんであろうか．酸化ストレスにより生体を構成する分子，たとえば核酸，蛋白質，脂質などが酸化修飾を受け，構造変化をきたしたり，機能不全を起こす．とくに，脳神経のような分裂能力の乏しい細胞ではこのような酸化修飾分子を新しい細胞をつくること（再生）により排除できないため異常な構造をもつ分子が蓄積しやすい．たとえばアルツハイマー病の原因にかかわるAβの蓄積には脳内の酸化修飾分子の蓄積や，酸化ストレスの亢進が関与している可能性がある．ビタミンC，E，ポリフェノール類は抗酸化作用をもち，抗老化，抗老年病効果をもつと期待されているが，介入研究，とくにサプリメントの摂取が有効であったとの証明はなされていない．

■遺伝子発現制御作用

近年，食品由来成分，とくにポリフェノール類であるレスベラトロール[10]，カテキン[11]などが遺伝子の発現を制御し，老化，老年病を抑制することが報告され，注目を集めている．レスベラトロールは赤ワインに含まれ，昔から“フレンチパラドックス（フランス人はアルコール摂取量が多いのに動脈硬化性疾患が少ない）”の原因ではないかとされてきた．レスベラトロールの働きとして抗酸化作用のほかに，寿命遺伝子であるsirtuin familyを活性化することが報告され，さらに実験動物で寿命を延長させたり，インスリン耐性を増強したりすることが見出された．しかし，ヒトに対する長寿作用は確認されておらず，さらに，日本人はアルコール耐性が低いのでワインの多量摂取によるアルコール毒性の危険が高いため勧められない．

一般患者への指導はどうあるべきか

現在，科学的に実証された“認知症を防ぐ食生活”は存在しない．しかしながら疫学的研究，動物実験ともに適正な量の野菜の摂取が認知症予防に有効である可能性を示唆している．また，とくに認知症患者さんのなかには偏った食生活

を続けており，他からの指導，介入が必要な方がおられることも事実である．このような患者さんに対し，規則正しい食生活と適切な量の野菜の摂取を促すことは，摂取食品そのものの改善に加え，生活習慣全般の改善により認知症の予防あるいは進行防止につながる可能性がある．

おわりに

医食同源とは日本古来からの哲学であり，超高齢化社会を迎えた現在，予防医療，統合医療の重要性が高まっている．認知症を予防する食生活を科学的に検証することが今後の課題である．

文献

1) St George-Hyslop PH, Westaway DA. Alzheimer's disease. Antibody clears senile plaques. Nature 1999 ; 400 : 116-7.
2) Garcia-Alloza M, Borrelli LA, Rozkalne A, et al. Curcumin labels amyloid pathology in vivo, disrupts existing plaques, and partially restores distorted neurites in an Alzheimer mouse model. J Neurochem 2007 ; 102(4) : 1095-104.
3) Marambaud P, Zhao H, Davies P. Resveratrol promotes clearance of Alzheimer's disease amyloid-beta peptides. J Biol Chem 2005 ; 280(45) : 37377-82.
4) Rezai-Zadeh K, Shytle D, Sun N, et al. Green tea epigallocatechin-3-gallate (EGCG) modulates amyloid precursor protein cleavage and reduces cerebral amyloidosis in Alzheimer transgenic mice. J Neurosci 2005 ; 25(38) : 8807-14.
5) Ono K, Yoshiike Y, Takashima A, et al. Potent anti-amyloidogenic and fibril-destabilizing effects of polyphenols in vitro : implications for the prevention and therapeutics of Alzheimer's disease. J Neurochem 2003 ; 87(1) : 172-81.
6) Barberger-Gateau P, Raffaitin C, Letenneur L, et al. Dietary patterns and risk of dementia : the Three-City cohort study. Neurology 2007 ; 69(20) : 1921-30.
7) Dai Q, Borenstein AR, Wu Y, Jackson JC, Larson EB. Fruit and vegetable juices and Alzheimer's disease : the Kame Project. Am J Med 2006 ; 119(9) : 751-9.
8) Kreijkamp-Kaspers S, Kok L, Grobbee DE, et al. Effect of soy protein containing isoflavones on cognitive function, bone mineral density, and plasma lipids in postmenopausal women : a randomized controlled trial. JAMA 2004 ; 292(1) : 65-74.
9) Harman D. Aging : a theory based on free radical and radiation chemistry. J Gerontol 1956 ; 11(3) : 298-300.
10) Baur JA, Pearson KJ, Price NL. Resveratrol improves health and survival of mice on a high-calorie diet. Nature 2006 ; 444(7117) : 337-42.
11) Reznichenko L, Amit T, Youdim MB, Mandel S. Green tea polyphenol (-)-epigallocatechin-3-gallate induces neurorescue of long-term serum-deprived PC 12 cells and promotes neurite outgrowth. J Neurochem 2005 ; 93(5) : 1157-67.

*　　*　　*

砂糖(甘い菓子類)摂取の影響

自治医科大学附属さいたま医療センター 神経内科
大塚美恵子 *Otsuka, Mieko*

keyword
アルツハイマー病，高インスリン血症，
インスリン抵抗性，砂糖，菓子類

はじめに

2型糖尿病（T2DM）は世界的に急速に増加しており，全体的な運動不足と肥満の蔓延が拍車をかけている．T2DMはもはや中高年のたんなる疾患ではなく若年層においても現在，将来の健康を脅かす深刻な疾患とみなされている[1]．多くの疫学調査でT2DMはアルツハイマー病（AD）の発症と関連があるとされており[2,3,4]，さらに最近糖尿病をともなわない高インスリン血症も危険因子として注目されている[5]．

本稿では，AD患者の耐糖能異常と高インスリン血症の実態，食行動のなかでも砂糖（甘い菓子類）摂取との関連について調査した結果を中心に述べてゆく．

インスリンとアルツハイマー病に関する知見

インスリン受容体は脳に広く分布しており，とくに海馬に集中している．また，Frolichらの報告[6]ではAD患者の脳内インスリン受容体濃度が健常対照者に比較して増加している．これはインスリンシグナリングの欠乏を代償的に高めようとしているためと解釈されている．さらに，インスリン分解酵素Insulin-degrading enzyme（IDE）はアミロイドベータ蛋白(Aβ)の分解と除去に関連があり[7]，IDEはインスリンとの親和性が強いため高濃度のインスリンはIDEによるAβの分解を抑制し[7]，神経原線維を構成する重要な要素の一つであるタウ蛋白(τ)のリン酸化を増すとも報告されている．このようにインスリン調節異常はAβ沈着やτのリン酸化を増す[8]ことでAD発症にかかわっていると考えられる．したがって，インスリンとインスリン抵抗性の研究は，T2DMとADの関連を解明するのに期待される分野とみなされている．

アルツハイマー病患者の栄養学的問題点

ADと栄養の問題は糖尿病やインスリンに関する問題以外に，現在のところ以下の点に絞られてきている．まず，野菜・果物の摂取はADを予防し，ビタミンE，ビタミンCなどの抗酸化ビタミンが注目されている[9]．つぎに，魚の摂取はADを予防し，魚油に含まれるドコサヘキサエン酸(DHA；22：6 n-3)やエイコサペンタエン酸(EPA；20：5 n-3)などのn-3系多価不飽和脂肪酸（PUFA）の役割が注目されている[10]．第3に動脈硬化の危険因子である高ホモシステイン血症がADでも認められ，ビタミンB_6，ビタミンB_{12}，葉酸の欠乏との関連が注目されている．これらは酸化ストレス，慢性炎症，血管

Radiat Med (2007) 25:255–262
DOI 10.1007/s11604-007-0132-8

ORIGINAL ARTICLE

Direct comparison study between FDG-PET and IMP-SPECT for diagnosing Alzheimer's disease using 3D-SSP analysis in the same patients

Takashi Nihashi · Hiroshi Yatsuya
Kazumasa Hayasaka · Rikio Kato · Shoji Kawatsu
Yutaka Arahata · Katsushige Iwai · Akinori Takeda
Yukihiko Washimi · Kumiko Yoshimura
Kanako Mizuno· Takashi Kato · Shinji Naganawa
Kengo Ito

Received: December 19, 2006 / Accepted: February 23, 2007

Abstract
Purpose. The purpose of this study was to evaluate and compare the diagnostic ability of 2-[^{18}F]-fluoro-2-deoxy-D-glucose (FDG) positron emission tomography (PET) and *N*-isopropyl-*p*-^{123}I iodoamphetamine single photon emission computed tomography (IMP-SPECT) using three-dimensional stereotactic surface projections (3D-SSP) in patients with moderate Alzheimer's disease (AD).

Materials and methods. FDG-PET and IMP-SPECT were performed within 3 months in 14 patients with probable moderate AD. Z-score maps of FDG-PET and IMP-SPECT images of a patient were obtained by comparison with data obtained from control subjects. Four expert physicians evaluated and graded the glucose hypometabolism and regional cerebral blood flow (rCBF), focusing in particular on the posterior cingulate gyri/precunei and parietotemporal regions, and determined the reliability for AD. Receiver operating characteristic (ROC) curves were applied to the results for clarification. To evaluate the correlation between two modalities, the regions of interest (ROIs) were set in the posterior cingulate gyri/precunei and parietotemporal region on 3D-SSP images, and mean Z-values were calculated.

Conclusion. No significant difference was observed in the area under the ROC curve (AUC) between FDG-PET and IMP-SPECT images (FDG-PET 0.95, IMP-SPECT 0.94). However, a significant difference ($P < 0.05$) was observed in the AUC for the posterior cingulate gyri/precuneus (FDG-PET 0.94, IMP-SPECT 0.81). The sensitivity and specificity of each modality were 86%, and 97% for FDG-PET and 70% and 100% for IMP-SPECT. We could find no significant difference between FDG-PET and IMP-SPECT in terms of diagnosing moderate AD using 3D-SSP. There was a high correlation between the two modalities in the parietotemporal region (Spearman's $r = 0.82$, $P < 0.001$). The correlation in the posterior cingulate gyri/precunei region was lower than that in the parietotemporal region (Spearman's $r = 0.63$, $P < 0.016$).

T. Nihashi (✉) · K. Hayasaka · R. Kato
Department of Radiology, National Center for Geriatrics and Gerontology, 36-3 Gengo, Morioka-Cho, Ohbu 474-8522, Japan
Tel. +81-562-46-2311; Fax +81-562-48-2373
e-mail: dr284@hotmail.com

H. Yatsuya
Department of Pubic Health, Nagoya University School of Medicine, Nagoya, Japan

S. Kawatsu
Department of Radiology, Kyoritsu General Hospital, Nagoya, Japan

Y. Arahata · K. Iwai · A. Takeda · Y. Washimi
Department of Neurology, National Center for Geriatrics and Gerontology, Ohbu, Japan

K. Yoshimura · K. Mizuno · T. Kato · K. Ito
Department of Brain Science and Molecular Imaging, National Center for Geriatrics and Gerontology, Ohbu, Japan

S. Naganawa
Department of Radiology, Nagoya University Graduate School of Medicine, Nagoya, Japan

Key words 3D-SSP · Alzheimer's disease · SPECT · PET

Introduction

For the clinical diagnosis of Alzheimer's disease (AD), regional glucose metabolism and cerebral blood flow (rCBF) are measured by positron emission tomography (PET) and single photon emission computed tomography (SPECT), respectively. Several studies have reported that changes in the regional glucose metabolism or rCBF are useful for the diagnosis of AD.[1–8]

Recent computational advances have improved the detection of regional metabolic and perfusion change using three-dimensional stereotactic surface projections (3D-SSP) or statistical parametric mapping (SPM) for the clinical diagnosis.[9–16] These two methods use PET and SPECT to analyze an individual brain in comparison with a standard brain, after stereotactic normalization, pixel by pixel or voxel by voxel. Ishii et al. showed that the fully automatic diagnostic system, using 3D-SSP, was able to perform at a diagnostic level similar to that of the visual inspection of conventional axial images by experts using the glucose analog 2-[^{18}F]-fluoro-2-deoxy-D-glucose (FDG)-PET.[17] Imabayashi et al. showed that the ability of 3D-SSP to discriminate early AD patients from control subjects was superior to that of visual inspection.[14] Tang et al. reported that the addition of 3D-SSP to the transaxial section display of SPECT improved the reproducibility and the diagnostic performance of AD.[12]

In terms of a comparison between PET and SPECT, it is apparent that PET has the advantage of greater sensitivity and greater spatial resolution. SPECT is the most widely available modality for functional neuroimaging techniques to evaluate dementia. Because the availability of PET is limited, PET is not used as often as SPECT clinically. Recently, the use of 3D-SSP or SPM has enabled the diagnosis of AD with greater accuracy.

Few reports have made a direct comparison of the diagnostic ability between PET and SPECT using statistical brain mapping methods in the same patients. Therefore, the purpose of the present study is to compare the ability to discriminate an AD pattern from healthy subjects using a 3D-SSP analysis of FDG-PET and *N*-isopropyl-*p*-^{123}I iodoamphetamine (IMP)-SPECT with visual interpretation by four expert physicians.

Methods

Subjects

Informed consent was obtained from all subjects prior to their participation in this study, which was approved by the ethics committee at our institution. FDG-PET and IMP-SPECT were performed on 14 patients (6 men, 8 women) within at least 3 months. The mean age was 70.1 ± 8.5 years. These patients were diagnosed as having probable AD according to the National Institute of Neurological and Communicative Disorders and Stroke (NINCDS) and the Alzheimer's disease and Related Disorders Association (ADRDA) criteria. The mean score of the Mini-Mental State Examination (MMSE) for these patients was 18.8 ± 4.3. For the FDG-PET study, seven subjects (four men, three women; mean age 61.2 years) participated as normal controls (NC), and for the IMP-SPECT study, nine subjects (two men, seven women; mean age 70.1 years) participated as normal controls.

FDG-PET

An ECAT EXACT HR 47 PET camera (Siemens/CTI, Germany) was used, and imaging was performed using two-dimensional acquisition at 60 min after intravenous administration of ^{18}F-FDG (370 MBq). Before FDG-PET scanning, the subjects rested in a supine position with eyes closed in a quiet room. The collected data were reconstructed into 128 × 128 pixel image matrices. Tissue attenuation of annihilation photons was corrected by transmission scans using rotating ^{68}Ge/^{68}Ga line sources. The in-plane spatial resolution was 4.0 × 3.9 mm in full-width at half-maximum (FWHM). The patient fasted for at least 6 h prior to the examination. Normal glucose levels were confirmed prior to the PET scan.

IMP-SPECT

A total of 222 MBq (6 mCi) of ^{123}I-IMP (Nihon Mediphysics, Hyogo, Japan) was injected into an antecubital vein while the subjects rested in a supine position with eyes closed in a quiet room. A single blood sample was obtained from the brachial artery between 9 and 10 min after the ^{123}I-IMP administration. SPECT scanning was carried out between 15 and 45 minutes after injection using a two-head rotating GCA 7200DI gamma camera (Toshiba, Tokyo, Japan) fitted with low-energy, high-resolution collimators. The data were acquired in 128 × 128 matrices through a 18° rotation at an angle interval of 4°. The projection data were prefiltered through a Butterworth filter and reconstructed using a Ramp back-

Table 1. Normal database of FDG-PET and IMP-SPECT

Method	No.	Sex (M/F)	Age
FDG-PET	37	23/11	59.0
IMP-SPECT	18	7/F	69.9

FDG-PET, 2-[^{18}F]-fluoro-2-deoxy-D-glucose positron emission tomography; IMP-SPECT, *N*-isopropyl-*p*-^{123}I iodoamphetamine single photon emission computed tomography

projection filter. Chang's attenuation correction and scattering correction using the triple energy window method were applied to the reconstructed images. The in-plane spatial resolution was 11.1 mm in FWHM. The final image slices were set parallel to the orbitomeatal line and were obtained at an interval of 3.44 mm through the entire brain. The rCBF images were quantitated according to the IMP-ARG method.[18]

Statistical images (3D-SSP)

The original FDG-PET and IMP-SPECT data were analyzed by an iSSP (SSP; Nihon Mediphysics) program, which was modified based on the NEUROSTAT program (Dr. Minoshima, Department of Radiology and Bioengineering, University of Washington, Seattle, WA, USA). After rotation and centering of the data set, the original data were realigned to the bicommissural line (AC-PC) and transformed into a stereotactic standard Talairach space. The cortical peak activity was projected onto the brain surface, and the peak value was projected back and assigned to the originating surface pixel. The extracted data sets were displayed on eight different angles, including the lateral, medial, superior, inferior, anterior, and posterior views. With the 3D-SSP programs in NEUROSTAT, the pixel values were normalized to the whole brain, thalamus, pons, and cerebellum (Fig. 1). The pixel values of an individual's image were compared with a normal database that originated at our institution (Table 1). The normal database was built as follows: 18 normal subjects (7 men, 11 women; mean age 69.9 years) for IMP-SPECT and 37 normal subjects (23 men, 14 women; mean age 59.0 years) for FDG-PET.

Statistical analysis/visual interpretation

Four nuclear medicine physicians randomly interpreted FDG-PET images of 14 AD patients and 7 NCs and IMP-SPECT images of 9 NCs. The interpretation of each image was performed at separate sessions, respectively. The statistical analyses were conducted using the following procedure. Two areas of the brain, the posterior cingulate gyri/precunei and parietotemporal region in each image (which were determined as characteristic for AD in advance of the study) were evaluated.[9] The degree of reduction in glucose metabolism or rCBF were interpreted, and a score of 5 was assigned if the change was considered "apparent decrease," which is characteristic of AD. Accordingly, scores of 4 to 1 were assigned to the changes that were considered "probable decrease," "unclear," "probable not a decrease," and "apparently not a decrease," respectively. Then, the reliability was evaluated using five steps similar to the regional evaluation.

When laterality was observed in a visual interpretation, the evaluation of a regional change was performed as follows. The scores assigned to the right and left sides (of the brain) of FDG-PET were compared for each side of the brain, and the higher score was recorded as the case's FDG-PET score for the specific area of the brain. The side of the higher FDG-PET score was considered a regional finding, and the IMP-SPECT score of the same side was recorded as the case's IMP-SPECT score. If the right- and left-side FDG-PET scores were the same, the higher score in IMP-SPECT was recorded as the regional finding. In fact, there were no discrepancies between the FDG-PET scores and the IMP-SPECT images in terms of laterality.

Second, the ratings of four readers were pooled for each area and for each image. The ROC analysis was performed for the graphics presentation, and the area under the curve was calculated to express the diagnostic accuracy of each image and each area numerically. Confidence intervals (CIs) of the AUC were used to test the difference in overall diagnostic accuracy between the images, the upper and lower limits of which were calculated either by adding or subtracting the standard error of the AUC times 1.96 for 95% CI and 1.65 for 90% CI. Because our primary interest lies in the difference in the diagnostic ability of FDG-PET from IMP-SPECT, we did not compare the difference in the AUC between the areas of the brain and did not take multiplicity in comparison into account. $P < 0.05$ was considered statistically significant. The statistical analyses were conducted using SPSS for Windows.

Correlation between FDG-PET and IMP-SPECT

To assess the agreement between two modalities, ROIs were set in the posterior cingulate gyri/precunei and parietotemporal region on 3D-SSP images, of which the pixel values were normalized to the whole brain bilaterally (Fig. 2). Then the mean Z-values of the right and left hemisphere were summed and used for analysis. We calculated kappa (κ) statistics, the proportion of concordance, and the Spearman's correlation coefficients of

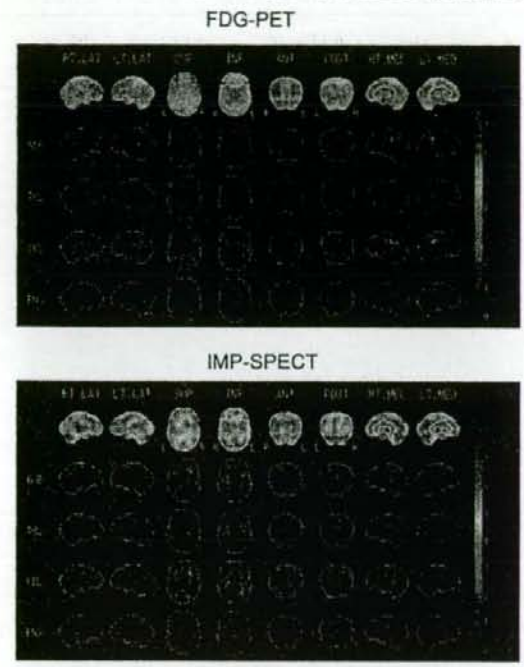

Fig. 1. Z-score images of three-dimensional stereotactic surface projections (3D-SSP) are shown from a representative Alzheimer's disease (AD) patient. These images demonstrate a decrease in the glucose metabolism and regional cerebral blood flow (rCBF). *Upper panel*: 2-[^{18}F]-Fluoro-2-deoxy-D-glucose positron emission tomography (FDG-PET). *Lower panel*: *N*-Isopropyl-*p*-^{123}I iodoamphetamine single photon emission computed tomography (IMP-SPECT). The extracted data sets are displayed on eight different angles, including the lateral (*RT LAT, LT LAT*), medial (*RT MED, LT MED*), superior (*SUP*), inferior (*INF*), anterior (*ANT*), and posterior (*POST*) views. With the 3D-SSP programs in NEUROSTAT, the pixel values are normalized to the whole brain (*GLB*), thalamus (*THL*), cerebellum (*CBL*), and pons (*PNS*)

Z-values in each area (the posterior cingulate gyri/precunei and parietotemporal region). For assessing κ statistics and the proportion of concordance, Z-values were first categorized according to their quartiles. Then the lowest quartile was considered as the "decrease" category. The κ statistic is defined as the agreement beyond chance divided by the amount of agreement possible by chance. As in most studies, $\kappa > 0.75$ was taken to represent excellent agreement beyond chance, 0.40–0.75 to mean fair agreement, and <0.40 to mean poor agreement.[19]

Results

Figure 3 shows the results of the clinical diagnosis of AD by 3D-SSP. The AUC of FDG-PET was 0.952 ± 0.023, and that of IMP-SPECT was 0.935 ± 0.026. There was no significant difference between FDG-PET and IMP-SPECT. Table 2 shows the results of each interpreter and the sum as the diagnosis ability. The sensitivity and specificity of each modality were 86%, and 97% for FDG-PET and 70%, and 100% for IMP-SPECT, respectively (Table 3).

Table 2. Results of visual inspection of 3D-SSP by each interpreter

	FDG-PET		IMP-SPECT	
Interpreter	AUC	SE	AUC	SE
A	0.939	0.057	0.976	0.026
B	0.954	0.047	0.96	0.041
C	0.888	0.074	0.821	0.091
D	0.995	0.01	1	0
Sum	0.952	0.023	0.935	0.026

3D-SSP, three-dimensional stereotactic surface projections; AUC, area under the curve; SE, standard error

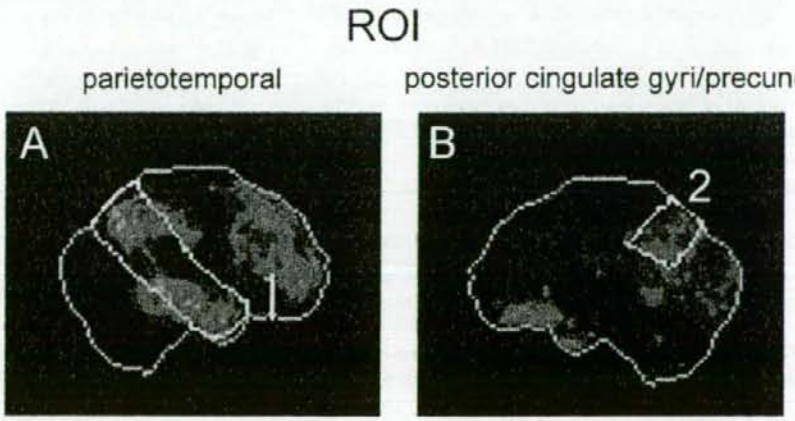

Fig. 2. Regions of interest (ROI) were set in the posterior cingulate gyri/precunei (**B**) and parietotemporal region (**A**) on 3D-SSP images of FDG-PET, in which the pixel values were normalized to the whole brain bilaterally

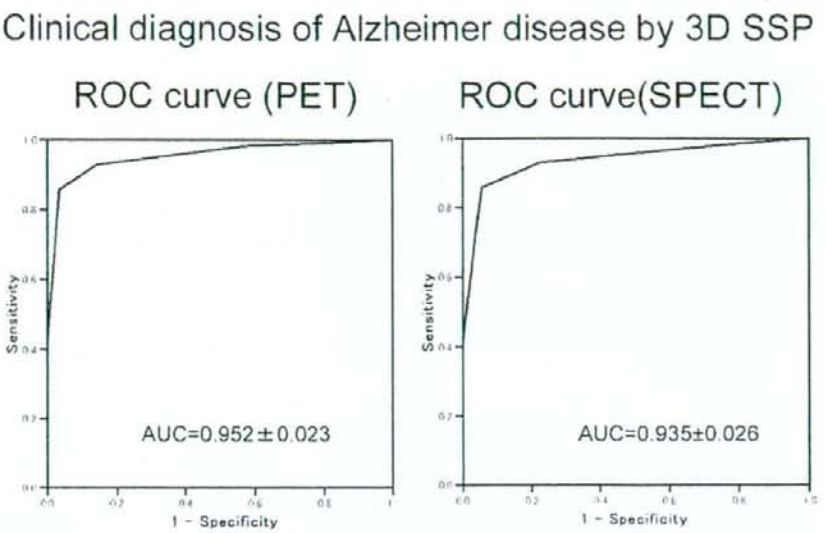

Fig. 3. Receiver operating characteristic (ROC) curves for clinical diagnosis of AD with visual inspection by experts. There was no significant difference between PET and SPECT. *AUC*, area under the curve

Table 3. Results of visual inspection of 3D-SSP by each interpreter: sensitivity and specificity

Interpreter	FDG-PET		IMP-SPECT	
	Sensitivity (%)	Specificity (%)	Sensitivity (%)	Specificity (%)
A	93	100	64	100
B	79	100	79	100
C	86	86	64	100
D	86	100	71	100
Sum	344	386	278	400
Average	86	97	70	100

Figure 4 shows the regional evaluation of the posterior cingulate gyri/precuneus and the parietotemporal region. The AUC of FDG-PET was 0.935 ± 0.028, and that of IMP-SPECT was 0.807 ± 0.046 in the posterior cingulate gyri/precuneus. A significant difference between FDG-PET and IMP-SPECT was observed ($P < 0.05$). The AUC of FDG-PET was 0.871 ± 0.038, and that of IMP-SPECT was 0.802 ± 0.046 in the parietotemporal region. There was no significant difference between FDG-PET and IMP-SPECT detected for this region.

Interrater agreement among four nuclear medicine physicians was evaluated by intraclass correlation coefficient with the Spearman-Brown correction. For both PET and SPECT, the agreement in the ratings among four raters were high: PET 0.94, SPECT 0.96.

There was a high correlation of Z-values between FDG-PET and IMP-SPECT in the parietotemporal region (Spearman's $r = 0.82$, $P < 0.001$). The correlation of the two modalities in the posterior cingulate gyri/precunei region was lower than that in the parietotemporal region (Spearman's $r = 0.63$, $P < 0.016$). In terms of the proportion of concordance and κ statistics, there was a perfect agreement in the parietotemporal region (both 1.0, $P < 0.001$). The proportion of concordance in the posterior cingulate gyri/precunei region was comparable (0.71), but agreement beyond chance evaluated by the κ statistics was poor and not significantly greater than zero (0.15, $P = 0.57$).

Discussion

Voxel-based statistical mapping methods, such as 3D-SSP and SPM, have been reported to be useful when delineating AD individuals from normal subjects.[9–16,20,21] Honda et al showed that 3D-SSP enhanced the specificity of SPECT inspection by nuclear medicine physicians